

# Structural Control of Nanocrystal Superlattices Using Organic Guest Molecules

Yasutaka Nagaoka,<sup>†</sup> Ou Chen,<sup>†</sup> Zhongwu Wang,<sup>‡</sup> and Y. Charles Cao<sup>\*†</sup>

<sup>†</sup>Department of Chemistry, University of Florida, Gainesville, Florida 32611, United States

<sup>‡</sup>Cornell High Energy Synchrotron Source (CHESS), Wilson Laboratory, Cornell University, Ithaca, New York 14853, United States

**S** Supporting Information

**ABSTRACT:** We report a host–guest chemistry approach to controlling the structures of nanocrystal superlattices through a molecular inclusion process. Upon addition of an appropriate amount of guest molecules such as squalane, polyisoprene, and 4-cyano-4'-pentylbiphenyl into a nanocrystal suspension, the resulting nanocrystal superlattices adopted non-close-packed structures (e.g., from face-centered cubic to body-centered cubic) and changed their morphologies to form superparticles. Our mechanistic studies revealed that these guest molecules can strongly tailor the kinetic process in superlattice formation, resulting in the formation of non-close-packed nanocrystal superlattices. The insights gained in this study are not only important for making nanocrystal superlattices with desirable architectures but also open a new way of synthesizing novel organic/inorganic composite materials.

The inclusion of guest molecules into a host lattice through noncovalent forces such as van der Waals interactions,  $\pi$ – $\pi$  interactions, and hydrogen bonding is an ordinary phenomenon that takes place in the formation of molecular crystals.<sup>1</sup> Host–guest inclusion chemistry has been widely used to design and construct molecular crystals with desired physical and chemical properties for the needs of various applications, for example, host–guest crystals with noncentral symmetry for the use in second-harmonic generation and cocrystals containing active pharmaceutical ingredients for drug delivery and formulation.<sup>2,3</sup> As analogues of molecular crystals, three-dimensional (3D) nanocrystal (NC) superlattices are ordered assemblies comprising one or more types of NC building blocks.<sup>4,5</sup> To date, many small molecules and polymers have been used to mediate the assembly of colloidal NCs, resulting in the preparation of a variety of organic/inorganic nanocomposites that exhibit unique optical, magnetic, electric, catalytic, or mechanical properties.<sup>6–10</sup> However, because most of these organic/inorganic nanocomposites do not adopt a 3D-ordered structure [e.g., face-centered cubic (fcc)], little progress has been made to date in the structural control of 3D NC superlattices using host–guest inclusion chemistry.

Recently, two research groups found that solvent molecules can occupy the interstitial space in PbSe NC superlattices and that solvent vapor can be used to control the structure of these NC superlattices, leading to the formation of non-close-packed superlattice structures such as body-centered cubic (bcc).<sup>11,12</sup>

Here we report that high-boiling organic compounds can be used as guest molecules to tailor the structure and morphology of NC superlattices. The resulting host–guest NC superlattices are stable under high-vacuum conditions during transmission electron microscopy (TEM) observations. Our results show that the inclusion of guest molecules such as squalane, squalene, and polyisoprene can lead to the formation of non-close-packed single-component or binary NC superlattices as well as the formation of superparticles (i.e., supercrystalline collections of NCs in the form of particles<sup>13,14</sup>).

To study the effects of the inclusion of guest molecules in NC superlattices, we chose the PbSe NC superlattice and squalane as the model lattice and guest molecule, respectively. The PbSe NC building blocks used in this study were 8.3 nm oleate-functionalized PbSe NCs, which were synthesized according to a literature method.<sup>15</sup> The choice of squalane as a guest molecule was due to its low melting point, high boiling point, and strong affinity to the PbSe NC's oleate ligands via van der Waals interactions. In a typical experiment, PbSe NC assembly samples were prepared by drop-casting a toluene solution containing PbSe NCs (5  $\mu$ M) in the presence (or absence) of 1% squalane onto the surface of substrates, after which the NC solution was dried by natural evaporation at room temperature. The substrates used in this study included diamond (or silicon) substrates for small-angle X-ray scattering (SAXS) measurements and carbon-coated TEM grids supported on silicon substrates.

Our SAXS measurements showed that the PbSe NC assemblies made in the absence of squalane adopt an fcc superlattice structure. These NC assemblies displayed a SAXS pattern with eight peaks that could be indexed as the (111), (200), (220), (222), (331), (420), (422), and (333) Bragg diffractions of an fcc structure with a lattice constant ( $a$ ) of  $16.8 \pm 0.2$  nm (Figure 1a). In contrast, the PbSe NC assemblies prepared in the presence of squalane adopted a non-close-packed cubic superlattice structure whose SAXS pattern consisted of five peaks with normalized peak positions at  $q/q_0 \approx \sqrt{1}$ ,  $\sqrt{2}$ ,  $\sqrt{3}$ ,  $\sqrt{4}$ , and  $\sqrt{5}$ , identifying the crystalline domains as possessing a bcc structure with  $a = 13.9 \pm 0.1$  nm (Figure 1b). The structure identification of these two types of PbSe NC superlattices was further confirmed using TEM.

Under low-resolution TEM, both of these NC superlattices displayed cross-fringe images that were identified as the on-axis superlattice fringe patterns of the corresponding lattice

Received: September 26, 2011

Published: January 27, 2012

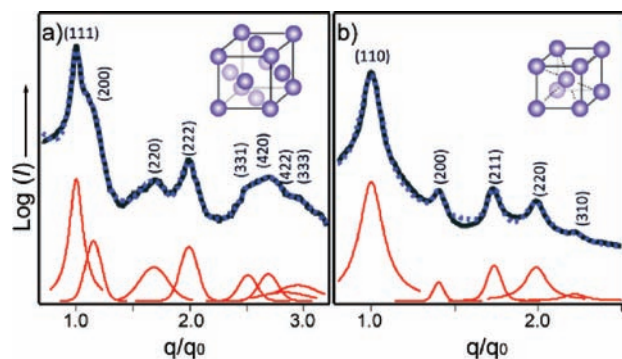


**Figure 1.** SAXS spectra of the (a) fcc and (b) bcc superlattices made of 8.3 nm PbSe NCs.

structures (Figure 2).<sup>16</sup> The assignment of the zone axis of these TEM images is consistent with the corresponding fast Fourier transform (FFT) patterns (Figure 2a–f, bottom left insets). Like the cross-fringes of atomic lattices imaged under high-resolution TEM, these superlattice fringe images were also acquired under objective-lens defocusing.<sup>16</sup> The origin of these superlattice fringes is likely from electron phase contrast due to the interference among the incident electron beam and small-angle diffraction beams through the supercrystalline NC assemblies.<sup>16</sup> Indeed, the appearance of superlattice fringes in TEM images follows the same selection rule that governs the systematic absence of Bragg reflections of atomic lattices with an identical symmetry. For example, an fcc NC superlattice displays lattice fringes from the corresponding scattering planes whose Miller indices ( $hkl$ ) are all odd or all even, whereas superlattice fringes from a bcc NC superlattice appear when the sum of the Miller indices of the corresponding plane is even (Figure 2).

The [100] image of the fcc superlattice (SL) shows the perpendicular cross-fringes projected from the  $\{020\}_{\text{SL}}$  and  $\{022\}_{\text{SL}}$  planes of the superlattice (Figure 2a), whereas that of the bcc superlattice displays cross-fringes projected from its  $\{011\}_{\text{SL}}$  and  $\{020\}_{\text{SL}}$  planes (Figure 2d). The cross-fringes in the [011] projection image of the fcc superlattice exhibit an angle of  $70.5^\circ$  (Figure 2c), which is consistent with the theoretically calculated value of  $70.53^\circ$  between the  $(\bar{1}11)_{\text{SL}}$  and  $(\bar{1}\bar{1}\bar{1})_{\text{SL}}$  planes (Figure 2b). On the contrary, the [110] image of the bcc superlattice shows the characteristic rectangular bcc cross-fringes from its  $(002)_{\text{SL}}$  and  $(\bar{1}10)_{\text{SL}}$  planes (Figure 2e). In addition, when viewed along the [111] zone axis, both the fcc and bcc NC superlattices show hexagonal cross-fringes, which are associated with the  $\{022\}_{\text{SL}}$  planes of the fcc structure but the  $\{011\}_{\text{SL}}$  planes of the bcc structure (Figure 2c,e). The lattice constants ( $a$ ) determined using these TEM images are  $17.0 \pm 0.3$  nm for the fcc PbSe NC superlattice and  $13.8 \pm 0.1$  nm for the bcc superlattice, in good agreement with the results of the SAXS measurements.<sup>17</sup>

The SAXS and TEM results unambiguously demonstrate that the presence of squalane significantly affects the assembly of PbSe NCs, leading to the formation of a bcc superlattice structure. The bcc PbSe NC superlattice has a lower particle packing density than the fcc structure formed without squalane (22.8% vs 24.8% of the volume occupied by inorganic PbSe cores in a unit cell).<sup>17</sup> The nearest interparticle distance in the bcc superlattice ( $a\sqrt{3}/2 = 12.0 \pm 0.1$  nm) is nearly identical to that in the fcc PbSe NC superlattice ( $a/\sqrt{2} = 12.0 \pm 0.2$  nm), and this distance corresponds to a nearest interparticle spacing

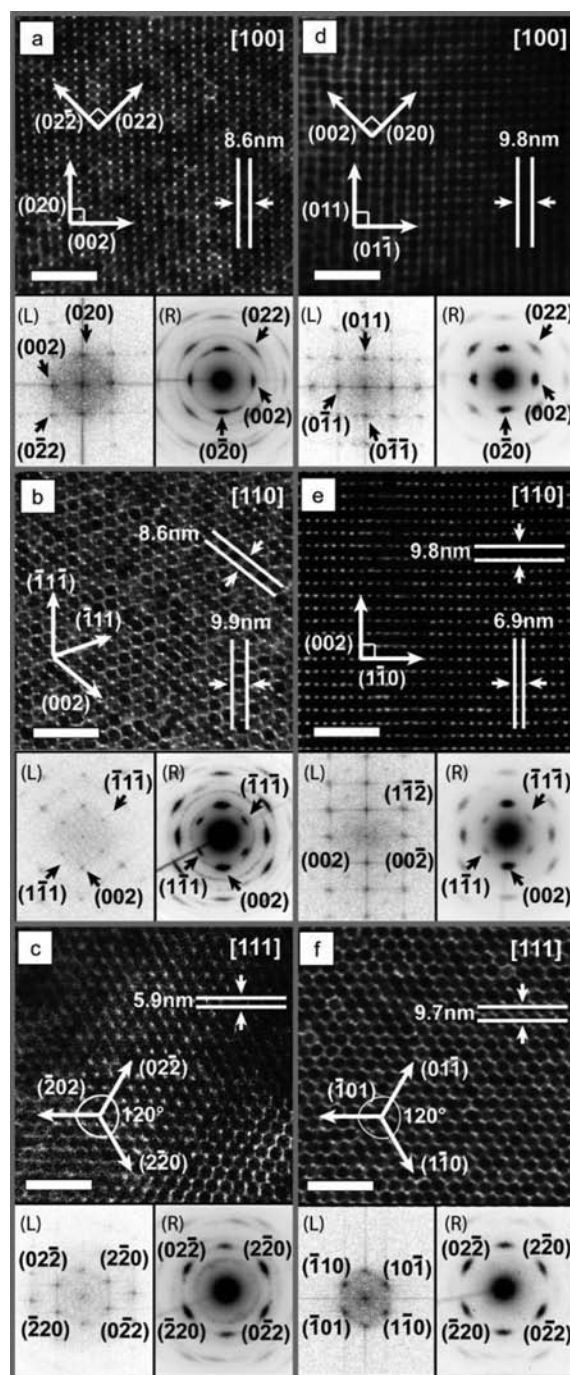
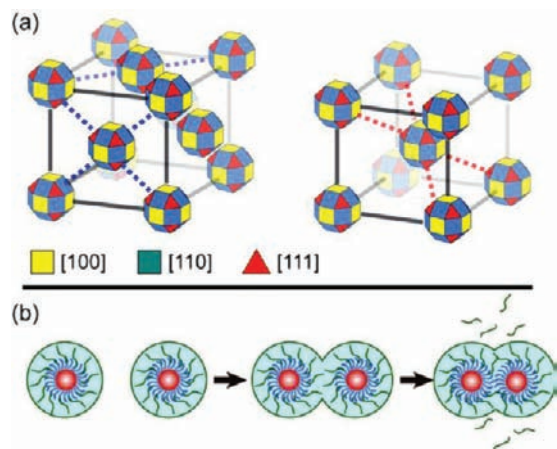


**Figure 2.** TEM images of the (a–c) fcc and (d–f) bcc NC superlattices. The left insets (L) are FFT patterns of the corresponding TEM images, and the right insets (R) are ED patterns from taken from the NC superlattices in the relevant projections. All of the scale bars are 100 nm.

of  $\sim 3.7$  nm,<sup>17</sup> in agreement with twice the length of an oleic acid molecule.<sup>12</sup> This result shows that squalane molecules may not occupy the space between nearest-neighbor PbSe NCs but instead occupy the void spaces such as the gaps between the second-nearest-neighbor PbSe NCs in the bcc structure. This structural configuration can maximize the energetic interactions between the NC building blocks in this non-close-packed structure, and the occupation of the interstitial void space with squalane molecules may further increase the stability of this superlattice structure.

Interestingly, when viewed along the same zone axis, the fcc and bcc PbSe NC superlattices display nearly identical dotlike electron diffraction (ED) patterns of a rock salt lattice (a type of fcc structure), suggesting that the individual PbSe NCs exhibit 3D-ordered atomic alignment within these superlattices (Figure 2a–f, bottom right insets).<sup>16,18</sup> In addition, the [100], [110], and [111] zone axes of the PbSe NCs in these superlattices are oriented coaxially with the corresponding superlattice zone axis (Figure 2), and thus, the 3D atomic orientations of the PbSe NCs are identical in the fcc and bcc superlattices. Such a 3D atomic alignment of PbSe NCs in superlattices requires a nonspherical interaction potential between neighboring NCs, indicating that the PbSe NCs made in this study may be nonspherical.<sup>12,15</sup> We propose that the shape of these PbSe NCs is a rhombicuboctahedron, a Wulff polyhedron enclosed by six  $\{200\}_{\text{NC}}$  faces, 12  $\{220\}_{\text{NC}}$  faces, and eight  $\{111\}_{\text{NC}}$  faces (Scheme 1a). This nearly

**Scheme 1. (a) Schematics of (left) fcc and (right) bcc Superlattices with Identical Coaxially Aligned PbSe NC Atomic Lattices; (b) Proposed Mechanism for NC Superlattice Formation**



spherical NC shape imposes nonspherical interparticle interaction potentials that allow the coaxial alignment of the atomic lattices of these NCs in a perfect geometric arrangement in both the fcc and bcc superlattices: the NCs are tightly packed in 12-fold coordination through their  $\{220\}_{\text{NC}}$  faces along the  $[110]_{\text{SL}}$  axes of the fcc superlattices, whereas when squalane is present, the NCs are tightly packed through their  $\{111\}_{\text{NC}}$  faces along the  $[111]_{\text{SL}}$  axes of the bcc superlattice with 8-fold coordination (Scheme 1a).

During bcc superlattice formation, squalane may affect both the thermodynamics and kinetics of the assembly of PbSe NCs during solvent evaporation. Squalane can be adsorbed onto the surface of PbSe NCs through van der Waals interactions and become a part of the solvent/ligand shell of these NCs in a toluene solution (Scheme 1b). During the formation of NC superlattices, the system must pay a large energetic penalty to remove squalane molecules from the surface of the NCs to maximize the NC packing density (Scheme 1b).<sup>17,19</sup> Thus, the formation of a bcc superlattice may be favored kinetically because the required energetic penalty is smaller than that for an fcc structure. In other words, this bcc superlattice likely is in a kinetically trapped state at a local free energy minimum. Indeed, the results of superlattice preparations in a partially closed evaporation chamber at a controlled temperature ( $20 \pm$

$0.5$  °C) are consistent with this mechanism (Figure S1 in the Supporting Information). Also, the unremoved squalane molecules can occupy the interstitial space of the bcc superlattice, which can substantially increase the lattice energy and stability of this non-close-packed structure.

In this mechanism, the guest molecule to be included into an NC superlattice should have a low melting point, as molecules with high melting points have a tendency to self-nucleate and thus leave the NC surface during solvent evaporation. For example, we did not obtain a bcc PbSe NC superlattice when octacosane was used as the guest molecule (Figure S2). The guest molecule's length is also important for the stability of the bcc superlattice. In comparison with shorter guest molecules, longer ones can more effectively fill the interstitial space of the superlattice (e.g., cross-linking the second-nearest-neighbor NCs in the lattice through hydrocarbon chain interdigitation) and thus result in a more stable inclusion superlattice. Indeed, the use of 1-octadecene as the guest molecule resulted in the formation of PbSe NC superlattices with a mixture of the fcc and bcc structures (Figure S3).

On the other hand, squalene is an unsaturated derivative of squalane with four trans double bonds, which makes its effective length slightly longer than that of squalane.<sup>20</sup> Instead of the flat bcc superlattice thin layers made in the presence of squalane, the inclusion of squalene resulted in PbSe NC superparticles of a bcc structure with sizes of 300–900 nm (Figure S4), indicating stronger interparticle interactions in the superparticles with squalene inclusion. In addition, Fourier transform IR spectra suggested that squalene indeed exists in the bcc PbSe NC superlattices, as indicated by the appearance of the characteristic vibrational bands associated with squalene (e.g., the  $\text{CH}_3$  asymmetric stretching vibration and the  $\text{CH}_3$  asymmetric and symmetric bending vibrations; see Figure S5).

Amazingly, with an even longer guest molecule, polyisoprene (MW  $\approx 400\,000$ ), we obtained 570 nm bcc PbSe superparticles with a relative size distribution ( $\sigma$ ) of 27% (Figure 3a–c). Moreover, the spontaneous formation of bcc PbSe superparticles upon solvent evaporation could also be introduced by the presence of 4'-pentyl-4-biphenylcarbonitrile (5CB), a widely used room-temperature nematic liquid-crystal material that exhibits strong  $\pi$ – $\pi$  interactions.<sup>21</sup> The resulting superparticles were 334 nm in diameter with  $\sigma = 20\%$  (Figure S6). The lattice constants of the bcc PbSe superparticles made with squalane, polyisoprene, and 5CB are identical to that of the bcc superlattice made with squalane (Table S1), showing that these guest molecules modify just the morphology of the bcc NC superlattice but not its structure.<sup>17</sup> This result is consistent with the proposed mechanism (Scheme 1), in which the energetic interactions between PbSe NCs also play a substantial role in the formation of the bcc superlattice.

Furthermore, to study the effects of squalane inclusion on binary NC superlattices, we used 4.8 nm Au and 9.2 nm  $\text{Fe}_3\text{O}_4$  NCs with an effective particle size ratio of 0.57. When the  $\text{Fe}_3\text{O}_4/\text{Au}$  NC ratio was 1:5, coassembly of these two types of NCs at room temperature resulted in  $\text{Fe}_3\text{O}_4/\text{Au}$  binary superlattices with  $\text{AlB}_2$  as the dominant structure (Figure 3d).<sup>22</sup> In this binary structure,  $\text{Fe}_3\text{O}_4$  NCs occupy the Al sites and Au NCs occupy the B sites. The superlattice exhibited a particle packing density of 22.9% and an effective space-filling factor of 72.0%.<sup>17</sup> In contrast, the presence of squalane led to the formation of binary  $\text{Fe}_3\text{O}_4/\text{Au}$  NC superlattices whose dominant structure was a cub- $\text{AB}_{13}$  superlattice, where B spheres occupy the vertices of the cuboctahedron.<sup>23</sup> The

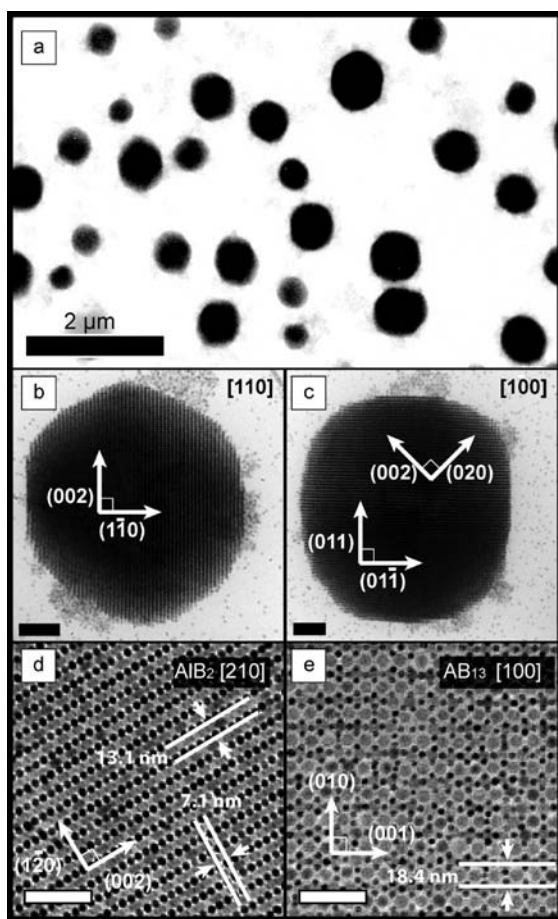


**Figure 3.** TEM images of superparticles made of (a–c) 8.3 nm PbSe NCs in the presence of polyisoprene and (d, e) binary superlattices made of 4.8 nm gold and 9.2 nm iron oxide NCs in the (d) absence and (e) presence of squalane. The scale bars are (a) 2  $\mu\text{m}$ , (b, c) 200 nm, and (d, e) 100 nm.

superlattice exhibited a volume packing density of 18.6% and an effective space-filling factor of only 65.4%.<sup>17</sup> This result clearly shows that guest-molecule inclusion stabilized the binary NC superlattice with a low space-filling factor, which may also have undergone a kinetically limited formation process.

In conclusion, we have reported an important study of the inclusion of guest molecules in NC superlattices. Our results show that guest-molecule inclusion leads to the formation of non-close-packed PbSe and binary  $\text{Fe}_3\text{O}_4/\text{Au}$  NC superlattices and enables control of the morphology of the NC superlattices, and we have synthesized PbSe NC superparticles having a bcc structure using squalene and polyisoprene. By means of guest-molecule inclusion, we have shown for the first time that both fcc and bcc NC superlattices with an identical 3D coaxially aligned NC atomic lattice can be prepared from identical PbSe NC building blocks. Moreover, one can expect to use guest molecules with specific optical, electronic, and magnetic properties to tailor the functionality of NC superlattices for applications such as biomedical diagnosis, solar cells, and photodetectors.

## ■ ASSOCIATED CONTENT

### Ⓢ Supporting Information

Detailed synthetic procedures, characterization techniques, calculations of the detailed structural information for the

superlattices, and additional TEM images. This material is available free of charge via the Internet at <http://pubs.acs.org>.

## ■ AUTHOR INFORMATION

### Corresponding Author

cao@chem.ufl.edu

## ■ ACKNOWLEDGMENTS

We thank the Major Analytical Instrumentation Center (MAIC) at the University of Florida for TEM usage. CHESS is supported by NSF Award DMR-0936384. Y.C.C. acknowledges the NSF (CAREER Award DMR-0645520) and the ONR (N00014-09-1-0441).

## ■ REFERENCES

- (1) Schwoerer, M.; Wolf, H. C. *Organic Molecular Solids*; Wiley-VCH: Weinheim, Germany, 2007.
- (2) Holman, K. T.; Pivovar, A. M.; Ward, M. D. *Science* **2001**, *294*, 1907.
- (3) Douglas, T.; Young, M. *Nature* **1998**, *393*, 152.
- (4) Murray, C. B.; Kagan, C. R.; Bawendi, M. G. *Science* **1995**, *270*, 1335.
- (5) Redl, F. X.; Cho, K. S.; Murray, C. B.; O'Brien, S. *Nature* **2003**, *423*, 968.
- (6) Suda, M.; Einaga, Y. *Angew. Chem., Int. Ed.* **2009**, *48*, 1754.
- (7) Chen, C. L.; Rosi, N. L. *J. Am. Chem. Soc.* **2010**, *132*, 6902.
- (8) Srivastava, S.; Kotov, N. A. *Acc. Chem. Res.* **2008**, *41*, 1831.
- (9) Chen, T.; Wang, H.; Chen, G.; Wang, Y.; Feng, Y. H.; Teo, W. S.; Wu, T.; Chen, H. Y. *ACS Nano* **2010**, *4*, 3087.
- (10) (a) Mann, S. *Nat. Mater.* **2009**, *8*, 781. (b) Sun, Z. C.; Bai, F.; Wu, H. M.; Schmitt, S. K.; Boye, D. M.; Fan, H. Y. *J. Am. Chem. Soc.* **2009**, *131*, 13594. (c) Xu, W.; Xue, X. J.; Li, T. H.; Zeng, H. Q.; Liu, X. G. *Angew. Chem., Int. Ed.* **2009**, *48*, 6849. (d) Huynh, W. U.; Dittmer, J. J.; Alivisatos, A. P. *Science* **2002**, *295*, 2425. (e) Jia, Q. X.; McCleskey, T. M.; Burrell, A. K.; Lin, Y.; Collis, G. E.; Wang, H.; Li, A. D. Q.; Foltyn, S. R. *Nat. Mater.* **2004**, *3*, 529. (f) Javier, A.; Yun, C. S.; Sorena, J.; Strouse, G. F. *J. Phys. Chem. B* **2003**, *107*, 435. (g) Dong, H.; Zhu, M.; Yoon, J. A.; Gao, H.; Jin, R.; Matyjaszewski, K. *J. Am. Chem. Soc.* **2008**, *130*, 12852. (h) Choi, J. J.; Bealing, C. R.; Bian, K. F.; Hughes, K. J.; Zhang, W. Y.; Smilgies, D. M.; Hennig, R. G.; Engstrom, J. R.; Hanrath, T. *J. Am. Chem. Soc.* **2011**, *133*, 3131.
- (11) Goodfellow, B. W.; Patel, R. N.; Panthani, M. G.; Smilgies, D. M.; Korgel, B. A. *J. Phys. Chem. C* **2011**, *115*, 6397.
- (12) Bian, K. F.; Choi, J. J.; Kaushik, A.; Clancy, P.; Smilgies, D. M.; Hanrath, T. *ACS Nano* **2011**, *5*, 2815.
- (13) Zhuang, J. Q.; Wu, H. M.; Yang, Y. A.; Cao, Y. C. *J. Am. Chem. Soc.* **2007**, *129*, 14166.
- (14) Zhuang, J. Q.; Wu, H. M.; Yang, Y. G.; Cao, Y. C. *Angew. Chem., Int. Ed.* **2008**, *47*, 2208.
- (15) Cho, K. S.; Talapin, D. V.; Gaschler, W.; Murray, C. B. *J. Am. Chem. Soc.* **2005**, *127*, 7140.
- (16) Fultz, B.; Howe, J. M. *Transmission Electron Microscopy and Diffractometry of Materials*, 3rd ed.; Springer: New York, 2007.
- (17) See the Supporting Information.
- (18) Talapin, D. V.; Murray, C. B. *Science* **2005**, *310*, 86.
- (19) Shah, P. S.; Holmes, J. D.; Johnston, K. P.; Korgel, B. A. *J. Phys. Chem. B* **2002**, *106*, 2545.
- (20) Tsvetkov, V. N. *Rigid-Chain Polymers*; Plenum: New York, 1989.
- (21) Lin, I.-H.; Miller, D. S.; Bertic, P. J.; Murphy, C. J.; de Pablo, J. J.; Abbott, N. L. *Science* **2011**, *332*, 1297.
- (22) Smith, D. K.; Goodfellow, B.; Smilgies, D. M.; Korgel, B. A. *J. Am. Chem. Soc.* **2009**, *131*, 3281.
- (23) Shevchenko, E. V.; Talapin, D. V.; O'Brien, S.; Murray, C. B. *J. Am. Chem. Soc.* **2005**, *127*, 8741.